Aeroacoustics Conferences
20-23 May 2019, Delft, The Netherlands
25th AIAA/CEAS Aeroacoustics Conference

10.2514/6.2019-2597

Streaks and coherent structures in jets from round and serrated nozzles

Georgios Rigas*, Ethan Pickering
California Institute of Technology, Pasadena, CA, USA
Oliver Schmidt
Mechanical Engineering, University of California, San Diego, La Jolla, CA USA
Petrônio A. S. Nogueira, André V. G. Cavalieri
Instituto Tecnológico de Aeronáutica, São José dos Campos, Brazil
Guillaume A. Brès
CASCADE Technologies, Palo Alto, CA, USA
Tim Colonius
California Institute of Technology, Pasadena, CA, USA

Hydrodynamic instabilities are directly related to large-scale coherent structures that are correlated with jet noise emission. Unravelling and accurately predicting their fundamental dynamics shows a promising direction for designing quieter jet engines. In this study, we analyze high-fidelity large-eddy simulation data of a turbulent Mach 0.4 round jet and a Mach 1.5 chevron jet. Using spectral proper orthogonal decomposition we identify, beyond the well-known[1] Kelvin–Helmoholtz and Orr mechanisms, elongated alternating streamwise streaks of high and low-speed fluid that have been associated with a non-modal lift-up effect in wall-bounded shear flows. In the global three-dimensional domain, the most energetic streaks manifest for azimuthal wavenumber $m = 1$ and frequency $St \to 0$. Furthermore, for the chevron jet, streaks and streamwise vortices appear due to the presence of the serrated nozzle, and they inherit the periodicity of the nozzle geometry. Finally, local (planar) spectral proper orthogonal decomposition is used to analyze the coherent structures of the chevron jet flow. Near the nozzle exit, antisymmetric and symmetric modes appear to be amplified and linked to the presence of the chevrons/streaks. Further downstream, the most energetic modes share similar characteristics to the ones observed in round jets.

I. Introduction

Instabilities of free shear layers are directly related to the presence of coherent structures in turbulence. These waves have been traditionally sought as modal solutions of the governing Navier–Stokes equations, and experiment and simulation data alike confirm the acoustic importance of coherent structures in the aft-angle radiation of high subsonic and supersonic jets.[2]

For parallel laminar shear flows, Rayleigh's criterion states that a necessary condition for hydrodynamic instability is the presence of an inflectional base flow. Squire's theorem states that two-dimensional disturbances are the first to become unstable and determine a critical Reynolds number for modal instability. In the case of free-shear flows, such as round jets with inflectional profiles, disturbances grow due to the Kelvin–Helmholtz (KH) instability over a range of frequencies and azimuthal mode numbers.

However, such shear flows also suffer non-modal[3,4] instabilities involving two- and three-dimensional disturbances, independent of the existence of inflectional points. For wall-bounded flows, these non-modal mechanisms are identified as the first disturbance growth mechanisms promoting transition in subcritical regimes. The lift-up[5–7] and the Orr[8] mechanisms both lead to transient growth of disturbances in shear flows.

*rigas@caltech.edu

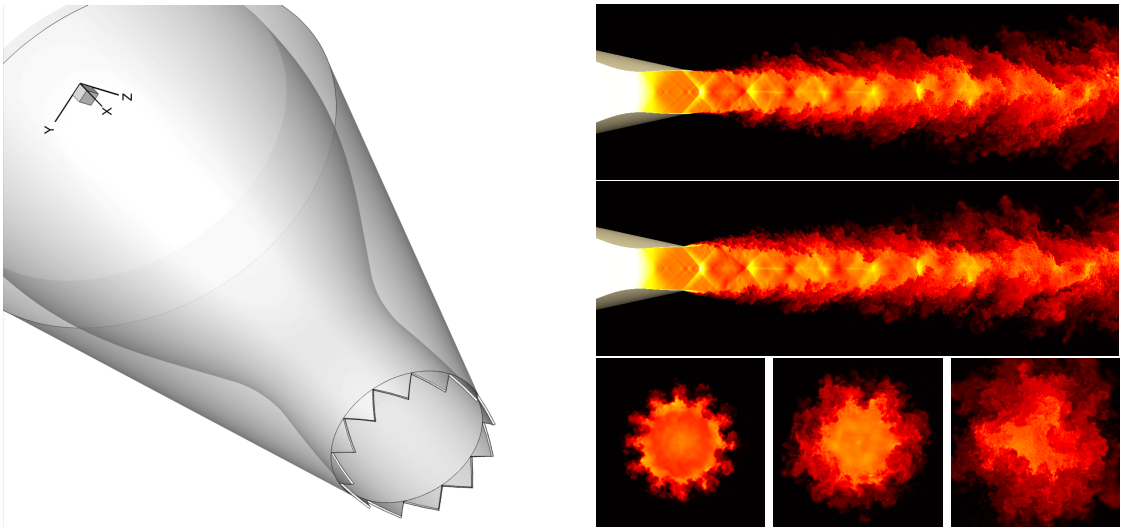

Figure 1. LES simulation of the Mach 1.5 chevron jet flow. Nozzle geometry with 12 chevrons (left). Instantaneous temperature fields T/T_∞ between 1 (black) and 2.2 (white) shown on the right; on a midsection plane at a chevron peak (top) and trough (middle); cross-flow cuts at x/D=1,2,5 (bottom).

For laminar jets, the effects of KH and Orr mechanism have been studied using linear resolvent analysis[9] and optimal temporal transient growth.[10] The amplification of steady streamwise perturbations (streaks) due to the vertical displacement of fluid particles by weak pairs of counter-rotating streamwise vortices through the lift-up mechanism has been studied in Ref. 11. More recently,[12] studied the stability of the KH instability in the presence of streaks and found that streaks have the ability to stabilize the KH instability for a plane laminar shear flow. A similar stabilizing mechanism has been identified in wall-bounded flows where the injection of streaks stabilizes the growth of Tollmien-Schlichting waves.[13] The lift-up mechanism has been studied also in compressible flows.[14,15]

For turbulent shear flows, instability mechanisms persist at high Reynolds numbers and appear to govern the dynamics of large-scale coherent structures according to a resolvent analysis of the turbulent mean flow field.[16,17] The recent resolvent analyses of a turbulent jet by Schmidt *et al.*[18] (and references therein) demonstrated the existence of both the KH and Orr mechanisms and showed how they control the observed large-scale structures and low-rank behavior in turbulent jets. The KH mode creates strong axisymmetric ($m = 0$) and helical ($m = 1$) perturbations over a range of frequencies peaking around $St \approx 0.6$. At higher frequencies, and for the axisymmetric mode at low frequencies ($St < 0.2$), where the KH response has lower gain, a different kind of instability termed Orr waves dominates the response. Nogueira *et al.*[19] showed that for very low frequencies, but higher azimuthal wavenumbers, the response consists of a third-kind of disturbances, elongated streamwise structures known as streaks, which, as mentioned above, have been associated with transition mechanisms in wall-bounded flows.

In this paper, we report evidence for the persistence of these mechanisms (KH, Orr, lift-up) at high Reynolds numbers and turbulent regimes for jet flows. The analysis is based on data obtained from high-fidelity Large Eddy Simulations (LES). Specifically, we focus on the streaks generated naturally in a round Mach 0.4 isothermal jet, and streaks that are associated with chevrons in a Mach 1.5 heated jet. In both cases, spectral proper orthogonal decomposition is employed to extract the coherent structures associated with these three-dimensional instability mechanisms.

II. Large-eddy simulations

The large eddy simulations (LES) are performed with the compressible flow solver "Charles" developed at Cascade Technologies.[20] The present version of the solver uses a novel mesh generation paradigm based on the computation of Voronoi diagrams.[21]

A. Mach 1.5 chevron jet

The chevron database is an extension of the previous work by Brès *et al.*,[22] with the flow configuration and nozzle geometry matching those of the experiment carried out at the United Technologies Research Center (UTRC) anechoic jet facility.[23] The operating conditions correspond to the supersonic heated ideally-expanded jet case B122 with the 12 count chevron (6 deg penetration) appended to the converging-diverging nozzle (see figure 1). The presence of the chevrons changes the nozzle-exit area and leads to the formation of shocks in the jet core. The Mach number is $M_j = U_j/c_j = 1.5$, the acoustic Mach number is $M_a = U_j/c_\infty = 1.98$ and the jet temperature is $T_j/T_\infty = 1.74$, where the subscripts j and ∞ refer to the fully-expanded jet properties and ambient (free-stream) conditions, respectively.

The main differences with the previous work are that wall modeling and near-wall adaptive mesh refinement are now employed on the internal nozzle surface, and that the simulated Reynolds number is now $Re_j = \rho_j U_j D/\mu_j = 0.95 \cdot 10^6$, matching the experimental value. This is done to better capture/model the state of the boundary layer inside the nozzle, which has been shown to be important for flow field and noise predictions.[24]

B. Mach 0.4 Round jet

The round jet database is an extension of the previous work by Brès *et al.*[24] for a contoured convergent-straight nozzle and was validated against companion experiments conducted at PPRIME Institute, Poitiers, France. Again, the simulation features near-wall adaptive mesh refinement and wall-modeling inside the nozzle, as well as synthetic turbulence to model the internal boundary-layer trip used in the experiment. This leads to fully turbulent nozzle-exit boundary layers. The jet is isothermal, with Mach number $M_j = M_a = 0.4$ and Reynolds number $Re_j = 4.5 \times 10^5$ matching the experimental values.

C. LES databases

The $M = 0.4$ database is the same as the one used in Ref. 18 and consists of 10,000 snapshots separated by $dtc_\infty/D = 0.2$ and interpolated onto a structured grid $x, r, \theta \in [0, 30] \times [0, 6] \times [0, 2\pi]$, with $656 \times 138 \times 128$ points in each direction. The points are equally-spaced in the azimuth direction to enable simple azimuthal decomposition in Fourier space.

The chevron database consists of 5,000 snapshots separated by $dtc_\infty/D = 0.1$ and interpolated onto a structured cylindrical grid $x, r, \theta \in [0, 30] \times [0, 5] \times [0, 2\pi]$, with $700 \times 142 \times 360$ points in each direction. Here, the resolution in the azimuthal direction was increased to capture the chevron effects.

Throughout this paper, the variables from both databases are reported as non-dimensionalized by time U_j/D, length D, velocity U_j, and pressure $\rho_j U_j^2$, with the resulting equation of state $p = \frac{\rho T}{\gamma M_j^2}$. Frequencies are expressed in Strouhal number, $St = fD/U_j$. Variables are reported by the vector

$$\boldsymbol{q} = [\rho, u_x, u_r, u_\theta, T]^T,$$

where a standard Reynolds decomposition separates the vector into mean, $\bar{\boldsymbol{q}}$, and fluctuating, $\boldsymbol{q}'$, components

$$\boldsymbol{q}(x, r, \theta, t) = \bar{\boldsymbol{q}}(x, r, \theta) + \boldsymbol{q}'(x, r, \theta, t).$$

Here, x, r, θ, correspond to the streamwise, radial and azimuthal directions, respectively.

D. Mean flow symmetries

For the round jet, the mean flow is axisymmetric respecting the continuous rotational symmetry of the nozzle geometry, $\overline{\boldsymbol{q}} = \overline{\boldsymbol{q}}_0(x, r)$.

Since the chevron jet has L-fold rotational symmetry (here $L = 12$ chevrons), the mean flow has to respect this symmetry:

$$\overline{\boldsymbol{q}}(x, r, \theta) = \overline{\boldsymbol{q}}_0(x, r) + \sum_{j \geq 1} \overline{\boldsymbol{q}}_{Lj}(x, r) e^{iLj\theta} + c.c.. \tag{1}$$

The mean velocity components for the chevron jet are shown in figure 2. Furthermore, each chevron sector exhibits mirror symmetry, which is reflected on the mean flow.

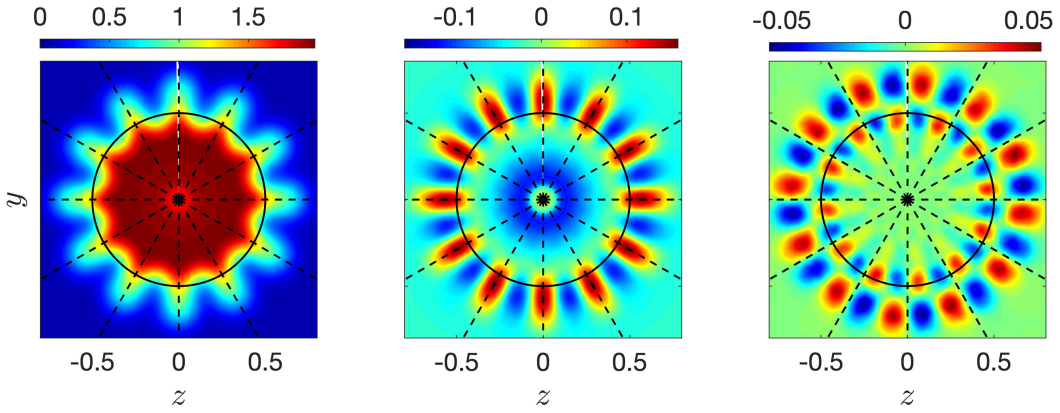

Figure 2. Mean velocity components in (x, r, θ) directions of the Mach 1.5 12-count serrated (chevron) nozzle at $x/D = 1.5$.

III. Methods

Spectral proper orthogonal decomposition (SPOD) is used to identify the most energetic coherent structures in the frequency domain. More details for the implementation can be found in Ref. 1

A. SPOD with continuous rotational symmetry (round jet)

Performing SPOD on turbulent flow data requires each timestep, t_k, to be represented as q_k and the entire dataset for N equally spaced timesteps is compactly assembled as

$$\mathcal{Q} = [q_1, q_2, ..., q_N]. \tag{2}$$

The data matrix $\mathcal{Q}$ is then azimuthally and temporally decomposed by a discrete Fourier Transform (DFT) to give the decomposed data matrices, $\mathcal{Q}_{m,\omega}$, by expanding

$$\mathbf{q}'(x, r, \theta, t) = \sum_{\omega} \sum_{m} \hat{\mathbf{q}}_{\omega,m}(x, r) e^{i\omega t + im\theta}. \tag{3}$$

Then, the cross-spectral density tensor at a given frequency is found by

$$\mathbf{S}_{m,\omega} = \mathcal{Q}_{m,\omega} \mathcal{Q}^*_{m,\omega} \tag{4}$$

and the SPOD eigenvalue problem is

$$\mathbf{S}_{m,\omega} \boldsymbol{W} \boldsymbol{\Psi}_{m,\omega} = \boldsymbol{\Psi}_{m,\omega} \boldsymbol{\Lambda}_{m,\omega}. \tag{5}$$

The SPOD modes are represented by the columns of $\boldsymbol{\Psi}_{m,\omega}$ and are ranked by the diagonal matrix of eigenvalues $\boldsymbol{\Lambda}_{m,\omega}$. The modes are orthonormal in the compressible energy norm[25]

$$\langle \boldsymbol{q}_1, \boldsymbol{q}_2 \rangle_E = \int\int\int \boldsymbol{q}_1^* diag\left(\frac{\bar{T}}{\gamma \bar{\rho} M^2}, \bar{\rho}, \bar{\rho}, \bar{\rho}, \frac{\bar{\rho}}{\gamma(\gamma - 1)\bar{T} M^2} \right) \boldsymbol{q}_2 r dx dr d\theta, \tag{6}$$

and satisfy $\boldsymbol{\Psi}^*_{m,\omega} \boldsymbol{W} \boldsymbol{\Psi}_{m,\omega} = \boldsymbol{I}$.

B. SPOD with discrete L-fold rotational symmetry (chevron jet)

Since the mean flow has L-fold rotational symmetry, it can be shown that the azimuthal Fourier modes of the fluctuating field have a sparse coupling.[26] That is, the fluctuating field can be separated into L independent "azimuthal orders", indexed by an equivalent Floquet multiplier M:

$$\mathbf{q}'(x, r, \theta, t) = \sum_{\omega} \sum_{M} \sum_{l} \hat{\mathbf{q}}_{\omega, M-Ll}(x, r) e^{i\omega t + i(M - Ll)\theta}. \tag{7}$$

$-\frac{L}{2} < M \leq \frac{L}{2}$	members: $m = M - Ll$								
	1	2	...	14	15	16	...	29	30
-5	-173	-161	...	-17	-5	7	...	163	175
...									
-1	-169	-157	...	-13	-1	11	...	167	179
0	-168	-156	...	-12	0	12	...	168	180
1	-179	-167	...	-23	-11	1	...	157	169
...									
6	-174	-162	...	-18	-6	6	...	162	174

Table 1. Symmetry groups with L-fold symmetry. Here $L = 12$.

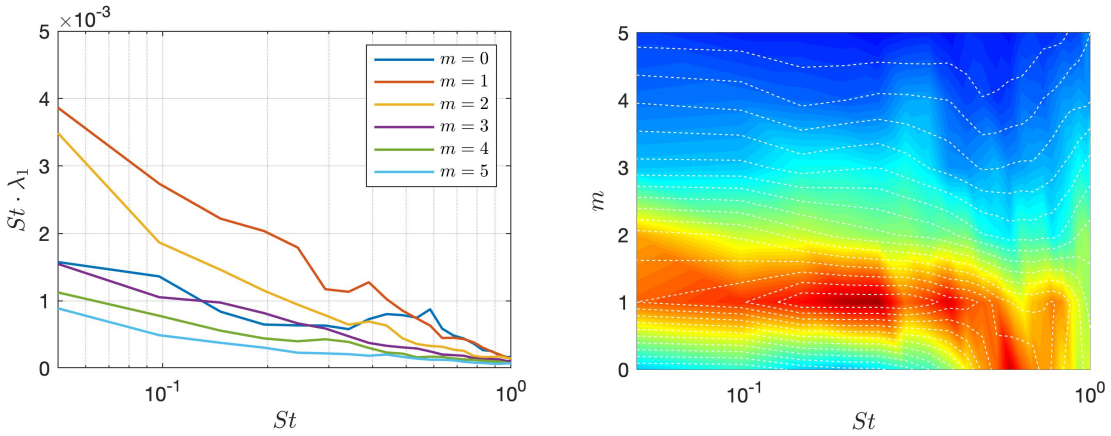

Figure 3. Mach 0.4 round jet. Energy of the first SPOD mode for the first six azimuthal wavenumbers and Strouhal numbers ranging from [0-1], plotted in a frequency premultiplied spectrum. The same plot is shown on the right recast as a percentage of the sum of energy at each azimuthal wavenumber.

The discrete counterpart of this expansion involves a finite set of modes with azimuthal wavenumbers $M - Ll$, for each M. For the specific case here, there are 360 uniformly distributed points in the azimuthal direction, resulting in the groups shown in table 1. Similar to the round jet, the cross-spectral density tensor at a given frequency is found now by combining together azimuthal modes within the group related to the azimuthal order M:

$$\mathbf{S}_{M,\omega} = \mathcal{Q}_{M,\omega}\mathcal{Q}^*_{M,\omega} \tag{8}$$

and the SPOD eigenvalue problem is

$$\mathbf{S}_{M,\omega}\boldsymbol{W}\boldsymbol{\Psi}_{M,\omega} = \boldsymbol{\Psi}_{M,\omega}\boldsymbol{\Lambda}_{M,\omega}. \tag{9}$$

IV. Streaks in round jets

In order to identify the most energetic coherent structure in the turbulent round jet, SPOD was performed over a range of Strouhal numbers, $[0, 1]$. Figure 3a shows, on a semi-log, frequency premultiplied plot, the energy of the first SPOD mode for azimuthal wavenumbers $m = 0$ to 5. This preserves the visual identification on the graph of areas of high energy, since the area under the power spectral density curve, $\Phi_m \equiv \lambda$, is proportional to the modal energy:

$$\langle \boldsymbol{q}_m, \boldsymbol{q}_m \rangle_E = \int_0^\infty \Phi_m \, \mathrm{d}St = \int_0^\infty St \; \Phi_m \; \mathrm{d}(\log St). \tag{10}$$

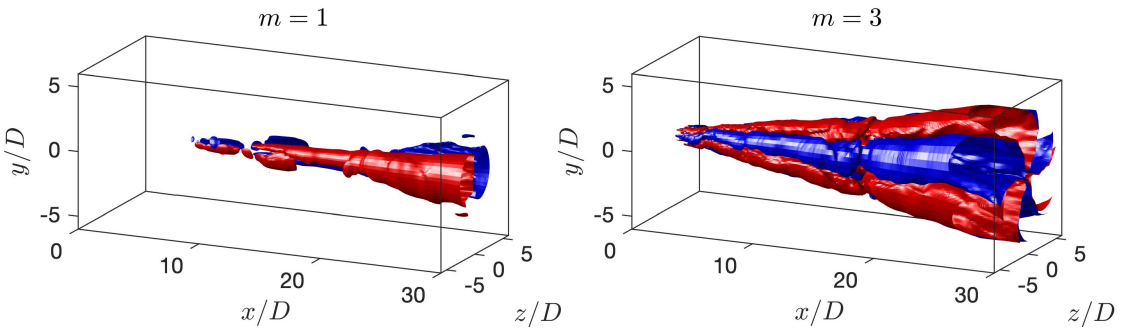

Figure 4. Mach 0.4 round jet. Three dimensional reconstruction of the first SPOD mode (axial velocity, u'_x) at $St \to 0$ for $m = 1$ (left) and $m = 3$ (right). Iso-contours of $\pm 25\%$ and $\pm 5\%$ of the maximum axial velocity are shown. High speed (red) and low speed (blue) streamwise elongated structures (streaks).

In figure 3b the same data are re-scaled at each frequency with the sum of energy over all azimuthal wavenumbers ($E_{m,St}/\sum_m E_{m,St} \times 100$). This highlights the dominant wavenumbers at each frequency and facilitates the identification of different instabilities. The importance of the Kelvin-Helmholtz mechanism for $m = 0$ near St=0.6, and its affect on nonzero azimuthal wavenumbers, is evident in both plots. At low frequencies, meaning $St \to 0$, for $m = 0$, the amplification of the KH mode diminishes and the Orr mechanism dominates. The modal shapes associated with the KH and Orr mechanisms have been shown in previous studies.[18] At the limit of small frequencies and mainly for $m = 1$ and 2, a second energetic region is observed. These trends in the wavenumber-frequency contour plots resemble those obtained for laminar boundary layers,[27] where lift-up dominates as streamwise wavenumbers approach 0, or equivalently the frequency approaches zero for spatially developing flows. For nonzero azimuthal wavenumbers, where the lift-up mechanism is expected to be found due to its three-dimensional characteristics, $m = 1$ provides the largest energy across all frequencies, followed by a gradual reduction for higher azimuthal wavenumbers.

In figure 4, the three-dimensional reconstructed streamwise velocity field from the leading SPOD mode is shown for zero frequency and $m = 1$ and 3. For $St \to 0$, and $m > 0$, the streamwise fluctuating velocity component was found to be the most amplified one. Here we approached $St \to 0$ using 1024 snapshots for the temporal FFT and 75% overlap, resulting in 36 realizations for the SPOD problem at each frequency and azimuthal wavenumber. Evidently, streamwise elongated structures, resembling streaks that have been observed in boundary layers,[27] are found, extending throughout the computational domain. These streaky structures are reminiscent of the dominant kinetic-energy-based structures educed by Freund & Colonius[28] using snapshot POD. Similar structures had been identified earlier by Citriniti George[29] performing local POD of the velocity field 3 diameters downstream of a round jet nozzle using a 172 hotwire array, but they had not been linked to the lift-up mechanism in the previous studies. Based on global energy, we find that the $m = 1$ streak is the most amplified one with spatial development downstream of the potential core where the shear layers merge. Streaks with higher azimuthal wavenumbers are identifier closer to the nozzle.

V. "Forced" steady streaks in chevron jets

Beyond the natural stochastic generation of streaks that could also occur in jets from serrated nozzles, we find that streaks are also formed directly due to the serrated nozzle geometry. In other words, the geometric characteristics of the periodic array of chevrons are "forcing" the amplification of streaks with the same azimuthal periodicity as the chevrons. Specifically, due to the generation of streamwise vorticity through the cross-stream velocity components (see figure 2), a large response is expected in the streamwise velocity component through a mechanism similar to the lift-up observed in round jets. Also, the chevrons lock the azimuthal angle of the streamwise vortices and streaks and make their identification in the turbulent field easier, when compared to the round jet. This is likely similar to turbulent boundary layers modified by a spanwise array of cylindrical elements, which develop steady streaks, in a process related to the spatial transient growth of upstream disturbances.[30]

In figure 5, iso-contours of mean streamwise vorticity and streamwise velocity are shown. The axisymmetric mean flow component has been subtracted from the second figure. Mean vorticity introduced due

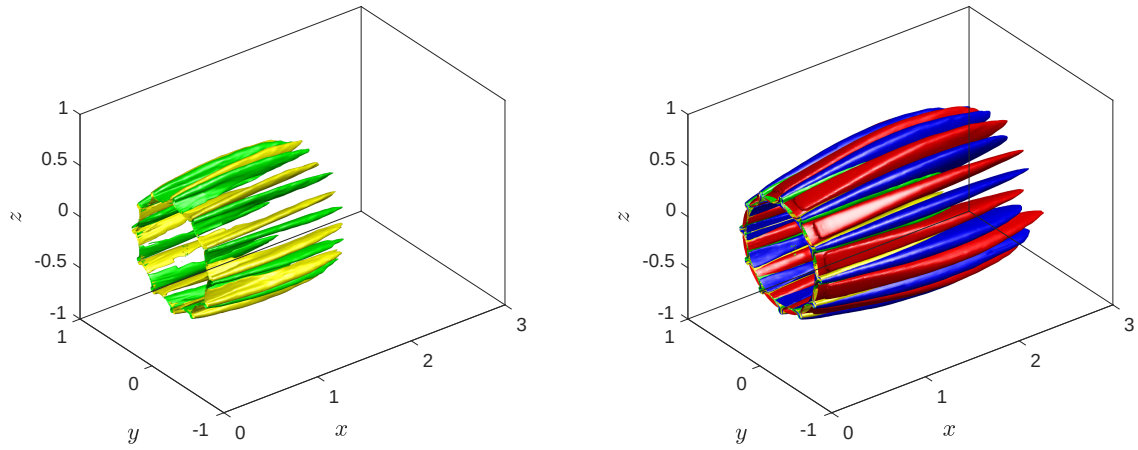

Figure 5. Mach 1.5 chevron jet. Iso-contours of mean streamwise vorticity for $\Omega_x = \pm 3.3$ (left) and mean streamwise velocity for $M_x = \pm 0.1$ (right). The axisymmetric mean flow has been subtracted for the second graph.

to the presence of chevrons creates streamwise vortices. Similar streamwise vortices have been identified before[31] either using chevrons or microjets in a Mach 0.9 turbulent jet. These streamwise vortices generate regions of high and low speed fluid, similar to the lift-up mechanism, amplifying transiently in space steady streaks as shown in figure 5b for the first few jet diameters in the streamwise direction. The presence of streamwise vortices in the upstream region continuously feeds streaks by the transport of momentum from inner or outer jet locations. Once streamwise vortices decay in amplitude, streaks reach their maximum amplitude, and subsequently decay downstream.

VI. Planar SPOD of chevron jet

Due to the presence of the chevrons, streamwise vortices and streaks are generated near the chevron nozzle. It is expected these structures to alter the stability characteristics of the coherent structures found in round jets. Because these features are local to the near-nozzle shear layer region, it is challenging to be identified using the global SPOD modes. To investigate them further, we preform a local SPOD problem in cross-stream planes at specific x locations. The most energetic $M = 0$, $St = 0.6$ mode in terms of fluctuating streamwise velocity is shown in figure 6. Here, we have truncated the expansion given in table 1 to include $m = \{-12, 0, 12\}$ for $M = 0$.

Preliminary results shown here, indicate that near the nozzle exit and approximately for the first 2 jet diameters, the most energetic mode is antisymmetric (sinuous) with major component the $m = \pm 12$ mode. In the same region, the second most energetic mode is symmetric (varicose) with major component again the $m = \pm 12$ mode. Beyond this, the quasi-axisymetric $m = 0$ mode becomes the dominant one. Three diameters downstream, the symmetric mode is the second most energetic, since the most energetic was found to be the axisymmetric. The third most energetic mode at this location is the symmetric one.

Based on the above, we see the presence of three distinct modes with specific symmetries and spatial structure. These correspond to azimuthal modes near the nozzle sharing the same periodicity with the chevron nozzle. There are two types of modes, one antisymmetric and a symetric one, with the antisymmetric being the most energetic locally near the nozzle. Further downstream the quasi-axisymmetric one becomes the prevailing mode, showing close similarities with the axisymmetric mode observed for the axisymmetric round jet. Future analysis will attempt to link these structures to the underlying instability mechanics and their link to the streaks introduced due to the presence of the chevrons.

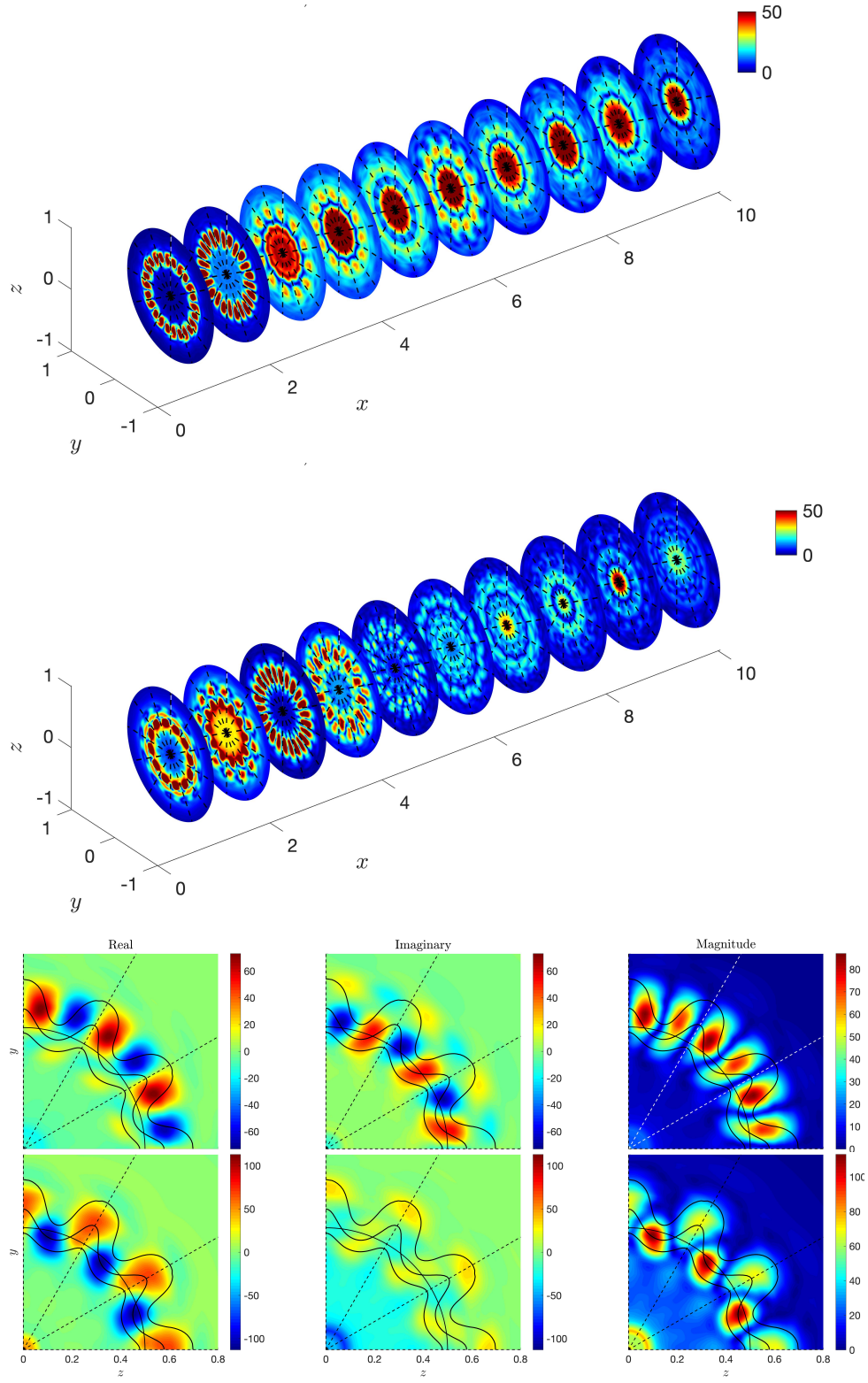

Figure 6. First and second most energetic planar SPOD mode for $M = 0$ ($m = [-12, 0, 12]$), $St = 0.6$: streamwise velocity perturbation. Magnitude of modes in physical space (top). Plane at $x/D = 1.5$ (bottom). Near the nozzle exit, the most energetic mode is antisymmetric (sinuous) with respect to the chevron geometry, and the second mode is symmetric (varicose). At 3 diameters from the nozzle, the quasi-axisymmetric mode becomes the dominant one.

VII. Conclusions

We have analyzed high-fidelity LES data of a turbulent Mach 0.4 round jet and a Mach 1.5 chevron jet. Using spectral proper orthogonal decomposition we identify, beyond the well-known[1] Kelvin-Helmoholtz and Orr modes, structures that take the form of elongated streamwise streaks that have been associated with non-modal lift-up mechanism in wall-bounded flows. In the global three-dimensional domain, the most energetic streaks manifest for azimuthal wavenumber $m = 1$ and frequency $St \to 0$. For the chevron jet, streaks and streamwise vortices appear due to the presence of the serrated nozzle, and they inherit the periodicity of the nozzle geometry. Finally, local (planar) spectral proper orthogonal decomposition is used to analyze the coherent structures of the chevron jet flow. Near the nozzle exit, antisymmetric and symmetric modes appear to be amplified and linked to the presence of the chevrons. Further downstream, the most energetic modes shares similar characteristics to the ones observed for round jets. A quantitative comparison in the future, will allow the clarification of the effect of the chevrons on the instability properties of the jet and the implications for acoustic radiation.

Acknowledgments

This research was supported in part by a grant from the Office of Naval Research (grant No. N00014-16-1-2445) with Dr. Steven Martens as program manager. The LES study was performed at Cascade Technologies, with additional support from NAVAIR, under the supervision of Dr. John T. Spyropoulos. The main LES calculations were carried out on DoD HPC systems in ERDC DSRC. G.R. and T.C. also acknowledge the support of the Boeing Company through a Strategic Research and Development Relationship Agreement CT-BA-GTA-1.

References

[1]Schmidt, O. T., Towne, A., Rigas, G., Colonius, T., and Brs, G. A., "Spectral analysis of jet turbulence," *Journal of Fluid Mechanics*, Vol. 855, 2018, pp. 953982.

[2]Jordan, P. and Colonius, T., "Wave packets and turbulent jet noise," *Annual Review of Fluid Mechanics*, Vol. 45, 2013, pp. 173–195.

[3]Schmid, P. J., "Nonmodal stability theory," *Annu. Rev. Fluid Mech.*, Vol. 39, 2007, pp. 129–162.

[4]Schmid, P. J. and Henningson, D. S., *Stability and transition in shear flows*, Vol. 142, Springer Science & Business Media, 2012.

[5]Moffatt, H., "The interaction of turbulence with strong wind shear," *Atmospheric Turbulence and Radio Waves Propagation, Proc. Intern. Collq. Moscow, 1965*, 1965, pp. 139–156.

[6]Ellingsen, T. and Palm, E., "Stability of linear flow," *The Physics of Fluids*, Vol. 18, No. 4, 1975, pp. 487–488.

[7]Landahl, M., "A note on an algebraic instability of inviscid parallel shear flows," *Journal of Fluid Mechanics*, Vol. 98, No. 2, 1980, pp. 243–251.

[8]Orr, W. M. F., "The stability or instability of the steady motions of a perfect liquid and of a viscous liquid." *Proc. R. Irish Acad. A*, 1907, pp. 69–138.

[9]Garnaud, X., Lesshafft, L., Schmid, P. J., and Huerre, P., "The preferred mode of incompressible jets: linear frequency response analysis," *Journal of Fluid Mechanics*, Vol. 716, 2013, pp. 189–202.

[10]Garnaud, X., Lesshafft, L., Schmid, P., and Huerre, P., "Modal and transient dynamics of jet flows," *Physics of Fluids*, Vol. 25, No. 4, 2013, pp. 044103.

[11]Jimenez-Gonzalez, J. I. and Brancher, P., "Transient energy growth of optimal streaks in parallel round jets," *Phys. Fluids*, Vol. 29, No. 11, 2017, pp. 114101.

[12]Marant, M. and Cossu, C., "Influence of optimally amplified streamwise streaks on the Kelvin–Helmholtz instability," *J. Fluid Mech.*, Vol. 838, 2018, pp. 478–500.

[13]Cossu, C. and Brandt, L., "Stabilization of Tollmien–Schlichting waves by finite amplitude optimal streaks in the Blasius boundary layer," *Physics of Fluids*, Vol. 14, No. 8, 2002, pp. L57–L60.

[14]Hanifi, A. and Henningson, D. S., "The compressible inviscid algebraic instability for streamwise independent disturbances," *Physics of Fluids*, Vol. 10, No. 8, 1998, pp. 1784–1786.

[15]Bakas, N. A., "Mechanisms underlying transient growth of planar perturbations in unbounded compressible shear flow," *Journal of Fluid Mechanics*, Vol. 639, 2009, pp. 479–507.

[16]McKeon, B. J. and Sharma, A. S., "A critical-layer framework for turbulent pipe flow," *Journal of Fluid Mechanics*, Vol. 658, 2010, pp. 336–382.

[17]Hwang, Y. and Cossu, C., "Linear non-normal energy amplification of harmonic and stochastic forcing in the turbulent channel flow," *J. Fluid Mech.*, Vol. 664, 2010, pp. 51–73.

[18]Schmidt, O. T., Towne, A., Rigas, G., Colonius, T., and Brès, G. A., "Spectral analysis of jet turbulence," *J. Fluid Mech.*, Vol. 855, 2018, pp. 953–982.

[19]Nogueira, P. A. S., Cavalieri, A. V. G., Jordan, P., and Jaunet, V., "Large-scale, streaky structures in turbulent jets," *in press, J. Fluid Mech.*, 2019.

[20]Brès, G. A., Ham, F. E., Nichols, J. W., and Lele, S. K., "Unstructured Large Eddy Simulations of Supersonic Jets," *AIAA*, Vol. 55, No. 4, 2017, pp. 1164–1184.

[21]Brès, G. A., Bose, S. T., Emory, M., Ham, F. E., Schmidt, O. T., Rigas, G., and Colonius, T., "Large eddy simulations of co-annular turbulent jet using a Voronoi-based mesh generation framework," AIAA paper 2018-3302, 2018.

[22]Brès, G. A., Nichols, J. W., Lele, S. K., Ham, F. E., Schlinker, R. H., Reba, R. A., and Simonich, J., "Unstructured Large Eddy Simulation of a Hot Supersonic Over-Expanded Jet with Chevrons," AIAA paper 2012-2213, 2012.

[23]Schlinker, R. H., Simonich, J. C., Reba, R. A., Colonius, T., Gudmundsson, K., and Ladeinde, F., "Supersonic Jet Noise from Round and Chevron Nozzles: Experimental Studies," AIAA Paper 2009-3257, 2009.

[24]Brès, G. A., Jordan, P., Jaunet, V., Le Rallic, M., Cavalieri, A. V., Towne, A., Lele, S. K., Colonius, T., and Schmidt, O. T., "Importance of the nozzle-exit boundary-layer state in subsonic turbulent jets," *Journal of Fluid Mechanics*, Vol. 851, 2018, pp. 83–124.

[25]Chu, B.-T., "On the energy transfer to small disturbances in fluid flow (Part I)," *Acta Mechanica*, Vol. 1, No. 3, 1965, pp. 215–234.

[26]Sinha, A., Gudmundsson, K., Xia, H., and Colonius, T., "Parabolized stability analysis of jets from serrated nozzles," *Journal of Fluid Mechanics*, Vol. 789, 2016, pp. 36–63.

[27]Monokrousos, A., Åkervik, E., Brandt, L., and Henningson, D. S., "Global three-dimensional optimal disturbances in the Blasius boundary-layer flow using time-steppers," *J. Fluid Mech.*, Vol. 650, 2010, pp. 181–214.

[28]Freund, J. B. and Colonius, T., "Turbulence and sound-field POD analysis of a turbulent jet," *International Journal of Aeroacoustics*, Vol. 8, No. 4, 2009, pp. 337–354.

[29]Citriniti, J. H. and George, W. K., "Reconstruction of the global velocity field in the axisymmetric mixing layer utilizing the proper orthogonal decomposition," *Journal of Fluid Mechanics*, Vol. 418, 2000, pp. 137–166.

[30]Pujals, G., Cossu, C., and Depardon, S., "Forcing large-scale coherent streaks in a zero-pressure-gradient turbulent boundary layer," *Journal of Turbulence*, , No. 11, 2010, pp. N25.

[31]Alkislar, M. B., Krothapalli, A., and Butler, G., "The effect of streamwise vortices on the aeroacoustics of a Mach 0.9 jet," *Journal of Fluid Mechanics*, Vol. 578, 2007, pp. 139–169.